

Reconstruction and interpretation of photon Doppler velocimetry spectrum for ejecta particles from shock-loaded sample in vacuum

Xiao-Feng Shi(石晓峰), Dong-Jun Ma(马东军), Song-lin Dang(党松琳), Zong-Qiang Ma(马宗强), Hai-Quan Sun(孙海权), An-Min He(何安民), and Pei Wang(王裴)

Citation: Chin. Phys. B, 2021, 30 (**6**): 066201. DOI: 10.1088/1674-1056/abd9b2
Journal homepage: http://cpb.iphy.ac.cn; http://iopscience.iop.org/cpb

What follows is a list of articles you may be interested in

Ejecta from periodic grooved Sn surface under unsupported shocks

Wen-Bin Liu(刘文斌), Dong-Jun Ma(马东军), An-Min He(何安民), Pei Wang(王裴)
Chin. Phys. B, 2018, 27 (**1**): 016202. DOI: 10.1088/1674-1056/27/1/016202

Influence of shockwave profile on ejecta from shocked Pb surface: Atomistic calculations

Guo-Wu Ren(任国武), Shi-Wen Zhang(张世文), Ren-Kai Hong(洪仁楷), Tie-Gang Tang(汤铁钢), Yong-Tao Chen(陈永涛)
Chin. Phys. B, 2016, 25 (**8**): 086202. DOI: 10.1088/1674-1056/25/8/086202

Dynamic strength behavior of a Zr-based bulk metallic glassunder shock loading

Yu Yu-Ying, Xi Feng, Dai Cheng-Da, Cai Ling-Cang, Tan Ye, Li Xue-Mei, Wu Qiang, Tan Hua
Chin. Phys. B, 2015, 24 (**6**): 066201. DOI: 10.1088/1674-1056/24/6/066201

Effect of grain size and arrangement on dynamic damage evolution of ductile metal

Qi Mei-Lan, Zhong Sheng, He Hong-Liang, Fan Duan, Zhao Li
Chin. Phys. B, 2013, 22 (**4**): 046203. DOI: 10.1088/1674-1056/22/4/046203

Reconstruction and interpretation of photon Doppler velocimetry spectrum for ejecta particles from shock-loaded sample in vacuum*

Xiao-Feng Shi(石晓峰)[1], Dong-Jun Ma(马东军)[1,†], Song-lin Dang(党松琳)[2], Zong-Qiang Ma(马宗强)[1], Hai-Quan Sun(孙海权)[1], An-Min He(何安民)[1], and Pei Wang(王裴)[1,3,‡]

[1] *Institute of Applied Physical and Computational Mathematics, Beijing* 100094, *China*
[2] *Jiangxi University of Applied Science, Nanchang* 330103, *China*
[3] *Center for Applied Physics and Technology, Peking University, Beijing* 100871, *China*

(Received 2 December 2020; revised manuscript received 5 January 2021; accepted manuscript online 8 January 2021)

The photon Doppler velocimetry (PDV) spectrum is investigated in an attempt to reveal the particle parameters of ejecta from shock-loaded samples in a vacuum. A GPU-accelerated Monte–Carlo algorithm, which considers the multiple-scattering effects of light, is applied to reconstruct the light field of the ejecta and simulate the corresponding PDV spectrum. The influence of the velocity profile, total area mass, and particle size of the ejecta on the simulated spectra is discussed qualitatively. To facilitate a quantitative discussion, a novel theoretical optical model is proposed in which the single-scattering assumption is applied. With this model, the relationships between the particle parameters of ejecta and the peak information of the PDV spectrum are derived, enabling direct extraction of the particle parameters from the PDV spectrum. The values of the ejecta parameters estimated from the experimental spectrum are in good agreement with those measured by a piezoelectric probe.

Keywords: ejecta, photon Doppler velocimetry, Monte–Carlo algorithm, light scattering

PACS: 62.50.Ef, 42.25.Dd, 42.79.Qx, 62.20.M– **DOI:** 10.1088/1674-1056/abd9b2

1. Introduction

The strong shock wave released from the metal–vacuum/gas interface may eject a great number of metal particles.[1–5] Most of these particles are of micrometer-scale in size. This phenomenon of ejecta, or microjetting, was first observed by Kormer *et al*. in a plane impact experiment in the 1950s.[5] Later, the researchers in Los Alamos National Laboratory studied the production of particle ejection using the PHERMEX radiographic facility.[6] In recent decades, extensive investigations on particle ejection have been performed because of its important role in many scientific and engineering fields, including explosion damage,[7] pyrotechnics,[8] and inertial confinement fusion.[9,10] Many experimental approaches have attempted to measure the ejection production, such as the Asay foil,[3,11] foam recovery,[12] piezoelectric probes,[4,13] Fraunhofer holography,[14,15] x-ray/proton radiography,[2,16] Mie scattering,[16,17] and photon Doppler velocimetry (PDV).[18–24] In these approaches, Asay foil and piezoelectric probe are mainly used to measure the particles' momentum distribution, x-ray and proton radiography describe the space density of ejecta, foam recovery collects the total ejected mass, and Fraunhofer holography and Mie scattering measure the particles' diameter. These approaches can only measure some of these ejecta parameters. To reveal the full particle field of ejecta, multiple measurement approaches must be equipped. However, in real-world conditions, these approaches are hard to apply simultaneously because of limitations on the experimental space or configuration. Recently, PDV has attracted considerable attention[20,21,24] owing to its ability to recover the total area mass and the distributions of particle velocity and diameter at the same time. In addition, the light path of PDV is rather concise and its application is convenient. In some complex experimental configurations, PDV may be the only approach that can measure the ejecta particles.

A standard PDV setup is shown in Fig. 1. The photodetector records a mixture of reference and backscattering light. The reference wave is in the carrier frequency, and the backscattering wave from ejecta particles has a shifted frequency due to the Doppler effect. The interference of the two light waves in the photodetector leads to temporal beats of light intensity. The beat signal consists of a large number of harmonics with different amplitudes and phases. The heterodyne signal may change according to variations in the particles' position and velocity. A discrete Fourier transform is applied to sweep the beats over time, giving a two-dimensional spectrogram on the "frequency/velocity–time" plane. In the spectrogram, the brightness of each point represents the corresponding spectral amplitude. The spectrogram is composed

*Project supported by the National Natural Science Foundation of China (Grant Nos. 11902043 and 11772065) and the Science Challenge Project (Grant No. TZ2016001).

†Corresponding author. E-mail: ma_dongjun@iapcm.ac.cn
‡Corresponding author. E-mail: wangpei@iapcm.ac.cn

© 2021 Chinese Physical Society and IOP Publishing Ltd

of the integral of all particles' scattering effects. Hence, interpreting the spectrogram in detail remains a challenging task.

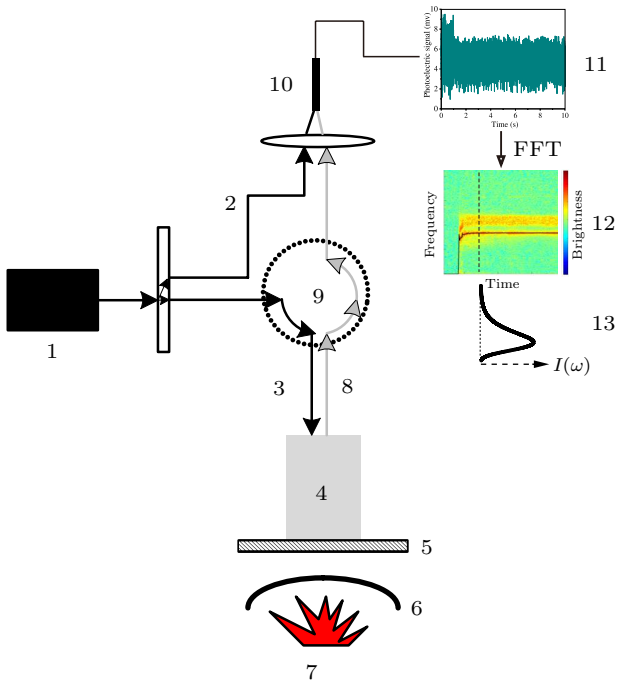


Fig. 1. Standard PDV setup: 1 laser; 2 reference light; 3 incident light; 4 ejecta; 5 metal plate; 6 shock; 7 detonation; 8 backscattering light; 9 optical circulator; 10 photodetector; 11 photoelectric signal; 12 PDV spectrogram; 13 instantaneous spectrum.

There have been several studies on the interpretation of the PDV spectrum. Buttler[25] used the spectrogram boundaries to determine the velocities of the spike and bubble of Richtmyer–Meshkov instability in loaded metal surface. The evolution of the PDV spectrogram in a gas environment was discussed by Sun *et al.*,[22] and the upper boundary of the spectrogram was used to obtain the particle size by considering aerodynamic deceleration effects. Fedorov *et al.*[23] discussed the influence of different particle sizes on the spectrogram boundary in further detail. Recently, Franzkowiak *et al.*[21] and Andriyash *et al.*[20,24] reconstructed the light field of ejecta and obtained the simulated PDV spectrum using single- and multiple-scattering theory, respectively. They varied the particles' parameters and fitted the simulated PDV spectrum to the experimental data. In this way, the particle velocity profile, diameter, and total area mass were recovered. Andriyash *et al.* considered the aerodynamic deceleration effects in a gas environment, whereas Franzkowiak *et al.* only discussed the case of a vacuum.

Franzkowaik *et al.*[21] and Andriyash *et al.*[20,24] proposed similar approaches for recovering the ejecta parameters from the PDV spectrum through reconstruction and then fitting. However, some assumptions were introduced in the reconstruction of the light field. Franzkowaik *et al.* assumed that only backscattering light was present, while Andriyash *et al.* set the light scattering direction to be uniform and random in space. These assumptions affect the accuracy of the spectrum reconstruction, and thus influence the recovery of the ejecta parameters. The fitting model is another factor that affects the interpretation of the PDV spectrum. Different convergence criteria may produce different results. The quantitative relationship between the ejecta parameters and the PDV spectrum remains unclear. Hence, it is difficult to obtain definite ejecta parameters from the PDV spectrum. These issues provide the motivation for the present work.

In this study, we improve the reconstruction method of the ejecta light field, and propose a novel model for extracting the ejecta parameters directly from the PDV spectrum. Mie theory, which gives a rigorous mathematical solution to Maxwell's equations, is applied to calculate the light scattering effects, and a Monte–Carlo (MC) algorithm is used to describe the light transport process realistically. This reconstruction method provides a high-fidelity simulation for the PDV spectrum. The procedure is discussed in detail in Section 2. The influence of the ejecta parameters on the PDV parameters is then explored through MC simulations in Subsection 3.1. In Subsection 3.2, we propose an optical model that reveals the relationships between the PDV spectrum characteristics and the ejecta parameters. With this model, the ejecta parameters can be extracted directly from the PDV spectrum, instead of fitting to experimental data. In Subsection 3.3, the estimated ejecta parameters from an experimental PDV spectrum are verified against those measured by a piezoelectric probe. Finally, the conclusions to this study are presented in Section 4.

2. Reconstruction of PDV spectrum

2.1. Theoretical background

The photodetector records reference and backscattering light waves. The scattering process of incident light is illustrated in Fig. 2. The scattering light from the ejecta is governed by the superposition of waves propagating in the ejection particles along different light paths i:

$$E_{\rm bs}(t) = \sum_i E_i(t), \tag{1}$$

where $E_{\rm bs}$ and E_i are the electric vectors of total and partial scattering waves, respectively.

The light intensity measured by the detector can be represented as

$$\begin{aligned} I(t) &= (E_r(t) + E_{\rm bs}(t))^2 = \left(E_r(t) + \sum_i E_i(t)\right)^2 \\ &= E_{\rm r}^2(t) + \sum_i E_i^2(t) + 2\sum_i E_{\rm r}(t) E_i(t) \\ &\quad + \sum_{i\neq j} E_i(t) E_j(t), \end{aligned} \tag{2}$$

where $E_{\rm r}^2$ and E_i^2 denote the intensity of the reference and scattering light signals, respectively. The third term represents the heterodyne beats between the reference and scattering light,

and the last term represents the heterodyne beats between the different scattering light paths. The Fourier transform of $I(t)$ is determined by the relation

$$\begin{aligned} I(\omega) &= \int \mathrm{d}t \exp(\mathrm{i}\omega t) I(t) \\ &\approx \int \mathrm{d}t \exp(\mathrm{i}\omega t) \left(2\sum_i E_\mathrm{r}(t) E_i(t)\right) \\ &= 2|E_\mathrm{r}| \cdot \sum_i |E_i| \Big|_{\omega=\omega_i-\omega_\mathrm{r}}, \end{aligned} \tag{3}$$

where $|E|$ is the amplitude of the light wave field. In Eq. (3), only the third term appearing in Eq. (2) remains. This is because the frequencies of the first two terms are too high to be measured by the detector and the value of the last term is much smaller than that of the third term. ω_r is the carrier frequency, and ω_i is the Doppler-shifted frequency, which corresponds to a sequence of scattering events along path i:

$$\omega_i = \frac{\omega_\mathrm{r}}{c} \sum_k \left(\boldsymbol{n}^\mathrm{s}_{k,i} - \boldsymbol{n}_{k,i}\right) \boldsymbol{v}_{k,i}, \tag{4}$$

where c is the speed of light, $\boldsymbol{n}_{k,i}$ and $\boldsymbol{n}^\mathrm{s}_{k,i}$ are the directions of wave propagation before and after scattering by particle k, and $\boldsymbol{v}_{k,i}$ is the velocity of this particle.

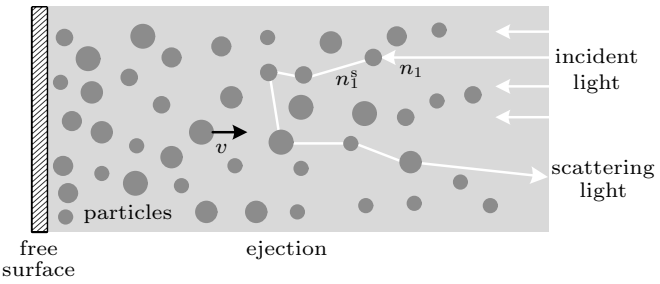


Fig. 2. Multiple scattering of light waves in ejection particles.

To reconstruct the PDV spectrogram [Eq. (3)], the key is to obtain $|E_i|$ and ω_i, *i.e.*, the detailed scattering process in the particles. For multiple-particle systems, the scattering field can be described by the transport equation[26,27]

$$\begin{aligned} &\left(\boldsymbol{n}\frac{\partial}{\partial r} + \sigma_s + \kappa\right) I(\boldsymbol{r}, n, t) \\ &= \int \left\langle \sigma_s p(\boldsymbol{n}, n') \exp\left(\mathrm{i}k_0 (\boldsymbol{n} - n') \boldsymbol{v}t\right) \right\rangle I(\boldsymbol{r}, n', t)\, \mathrm{d}\boldsymbol{n}', \end{aligned} \tag{5}$$

where I is the light intensity in the field, which depends on both the detection position $\boldsymbol{r}$ and the direction $\boldsymbol{n}$. σ_s and κ are the coefficients of scattering and absorption, respectively. $p(\boldsymbol{n}, n')$ is the scattering phase function. The right-hand side of this equation represents the contributions of scattering light from other positions.

At the boundaries of the ejection, the light intensity has the form

$$\begin{cases} I(\boldsymbol{r}=0, \boldsymbol{n}=\boldsymbol{n}_0, t) = I_0, \\ I(\boldsymbol{r}=0, \boldsymbol{n}=-\boldsymbol{n}_0, t) = I_\mathrm{bs} = (\sum_i |E_i|)^2, \end{cases} \tag{6}$$

where $\boldsymbol{n}_0$ is the direction of incident light, which is usually perpendicular to the free surface. I_0 and I_bs are the intensities of incident light and backscattering light, respectively, which correspond to the input and output of the transport equation.

2.2. Monte–Carlo algorithm

Andriyash *et al.*[20,24] used the discrete ordinate method to solve the transport equation [Eq. (5)]. In this paper, a more convenient and accurate method of the MC algorithm is applied to calculate the scattering effects. Compared with the discrete ordinate method, MC algorithm transform the complex light transport problem into multiple photons scattering problem. The detail scattering process can be considered in MC algorithm.

In the MC algorithm, the incident light is assumed to be a great number of photons. When passing through random granular media, only part of the photons can penetrate. The proportion of permeable photons is approximated by Beer–Lambert's law[17]

$$p_\mathrm{r} = \exp(-\tau L), \tag{7}$$

where L is the thickness of the medium and τ denotes the inverse extinction length, given by

$$\tau = N K_\mathrm{ext} \bar{A} = \frac{\sum_i (\pi/4) d_i^2 \cdot K_\mathrm{ext}(d_i)}{A_\mathrm{s} L}, \tag{8}$$

where N is the number of particles per unit volume, K_ext is the light extinction coefficient (determined by the particle diameter, light wavelength, and metal relative refraction index), $\bar{A}$ is the mean cross-section area of the particles, d_i is the diameter of particle i, and A_s is the light exposure area.

For particles in the light exposure area, the total mass has the form

$$m_0 A_\mathrm{s} = \sum_i \frac{1}{6} \pi d_i^3 \rho_0, \tag{9}$$

where m_0 is the total area mass of ejection and ρ_0 is the density of the particle material.

Combining Eqs. (8) and (9), we can rewrite Eq. (7) as

$$p_\mathrm{r} = \exp\left(-\frac{3 m_0 \sum_i d_i^2 K_\mathrm{ext}(d_i)}{2\rho_0 \sum_i d_i^3}\right). \tag{10}$$

The photons staying in the medium are scattered or absorbed by particles. The probabilities of scattering and absorption are calculated by the formula

$$\begin{cases} p_\mathrm{s} = K_\mathrm{sca}/K_\mathrm{ext}, \\ p_\mathrm{a} = K_\mathrm{abs}/K_\mathrm{ext}, \end{cases} \tag{11}$$

where the scattering coefficient $K_{\rm sca}$ and the absorption coefficient $K_{\rm abs}$ are calculated by Mie theory[28] as

$$\begin{cases} K_{\rm ext} = \dfrac{2}{\alpha^2}\sum\limits_{n=1}^{\infty}(2n+1)\,{\rm Re}\,(a_n+b_n), \\ K_{\rm sca} = \dfrac{2}{\alpha^2}\sum\limits_{n=1}^{\infty}(2n+1)\left(|a_n|^2+|b_n|^2\right), \\ K_{\rm abs} = K_{\rm ext}-K_{\rm sca}, \end{cases} \tag{12}$$

where α is a dimensionless particle diameter parameter, $\alpha = \pi d/\lambda$, λ is the light wavelength, and a_n, b_n are Mie coefficients. It is clear that $p_{\rm s}+p_{\rm a}=1$.

If the photon is absorbed by particles, it will completely disappear and be converted into the particle's internal energy. If the photon is scattered, its propagation direction and frequency will change, as shown in Fig. 3. The phase function of the scattering angle θ is calculated by the formula

$$p(\theta) = \frac{\lambda^2}{2\pi K_{\rm sca}}(|S_1(\theta)|^2+|S_2(\theta)|^2), \tag{13}$$

where S_1 and S_2 denote the scattering intensity components in the perpendicular and parallel directions

$$\begin{cases} S_1(\theta) = \sum\limits_{n=1}^{\infty}\dfrac{2n+1}{n(n+1)}\left(a_n\dfrac{{\rm dP_n}(\cos\theta)}{{\rm d}\cos\theta}+b_n\dfrac{{\rm dP_n^{(1)}}(\cos\theta)}{{\rm d}\theta}\right), \\ S_2(\theta) = \sum\limits_{n=1}^{\infty}\dfrac{2n+1}{n(n+1)}\left(a_n\dfrac{{\rm dP_n^{(1)}}(\cos\theta)}{{\rm d}\theta}+b_n\dfrac{{\rm dP_n}(\cos\theta)}{{\rm d}\cos\theta}\right), \end{cases} \tag{14}$$

where ${\rm P}_n$ and ${\rm P}_n^{(1)}$ are Legendre and first-order associative Legendre functions, respectively.

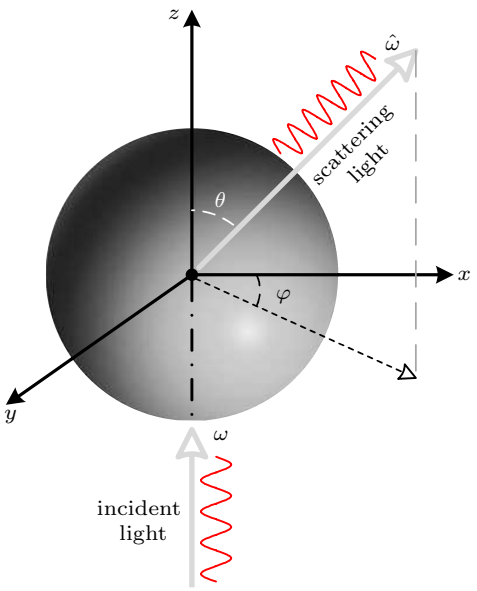


Fig. 3. Light scattering on a particle.

The incident light is assumed to be non-polarized, so the azimuth angle φ after scattering obeys the uniform random distribution

$$p(\varphi) = \frac{1}{2\pi}. \tag{15}$$

After scattering, the scattering angle and azimuth angle are added to the original light direction. The new direction cosine $\hat{u} = [\hat{u}_x, \hat{u}_y, \hat{u}_z]$ has the form

$$\begin{cases} \hat{u}_x = \dfrac{1}{\sqrt{1-u_z^2}}\sin(\theta)\,[u_x u_y\cos(\varphi)-u_y\sin(\varphi)] \\ \qquad +u_x\cos(\theta), \\ \hat{u}_y = \dfrac{1}{\sqrt{1-u_z^2}}\sin(\theta)\,[u_x u_z\cos(\varphi)-u_x\sin(\varphi)] \\ \qquad +u_y\cos(\theta), \\ \hat{u}_z = -\sin(\theta)\cos(\varphi)\sqrt{1-u_z^2}+u_z\cos(\theta), \end{cases} \tag{16}$$

where $u = [u_x, u_y, u_z]$ is the original direction cosine. When $|u_z| \approx 1$, the direction cosine $\hat{u}$ is calculated by the formula

$$\begin{cases} \hat{u}_x = \sin(\theta)\cos(\varphi), \\ \hat{u}_y = \sin(\theta)\sin(\varphi), \\ \hat{u}_z = \cos(\theta)\,u_z/|u_z|. \end{cases} \tag{17}$$

After scattering, the frequency of the photon will have changed. The new frequency of scattering light has the form

$$\hat{\omega} = \omega\left(1+\frac{\hat{v}-v}{c}n\right), \tag{18}$$

where v is the velocity of the last particle that the photon left, $\hat{v}$ is the current particle velocity, n is the photon direction, and ω is the photon frequency before scattering.

After passing through the entire ejection layer, few photons reach the free surface. An ideal diffuse reflection is assumed for these photons. After reflection, the space angles θ and φ are uniformly random in $[\pi/2, \pi]$ and $[0, 2\pi]$, respectively.

Because the ejection is blocked by the free surface, eventually all the photons are either absorbed by particles or backscattered out from the top of the ejection. The frequency shifts of these "out" photons are summarized as the theoretical PDV spectrogram:

$$I(\omega) \propto \sum_i |E_i| = \sum_i \sqrt{I_i} = n_{\rm out}|_{\omega=\hat{\omega}-\omega_{\rm r}} \cdot \sqrt{\frac{I_0}{n_0}}, \tag{19}$$

where n_0 is the number of initial photons and $n_{\rm out}$ is the distribution of out photons in terms of their frequency.

The detailed steps of the calculation procedure are as follows:

(i) First, the initial conditions of the photons and particles are set, such as the number and frequency of photons, and the diameter, velocity, and position of the particles. The photons start at the top of the ejection and then move towards the free surface.

(ii) The step sizes of all photons are set to the same and equal to one thousandth of the height of the ejecta.

(iii) In one iteration, all photons take one step in the direction of their propagation. Some photons may penetrate the

current ejection layer, and the proportion p_r is determined by Eq. (10). For each photon, a random number is generated in (0, 1). If the random number is less then p_r, the corresponding photon travels over the ejection layer boundary successfully. Otherwise, the corresponding photon is absorbed or scattered by particles in the ejection layer.

(iv) For the photons that remain in the ejection layer, we use Eq. (11) to determine whether they are scattered or absorbed. If the photon is scattered, the direction change is calculated by Eqs. (13)–(17). Because the phase function of the scattering angle is very complex, an acceptance–rejection method is applied. The new frequency of the scattered photons is determined by Eq. (18).

(v) Overall, if the photon travels across the ejection layer boundary, its position is updated; if the photon is scattered, its direction, frequency, and position are updated; if the photon is absorbed, it is labeled as such and removed from subsequent calculations.

(vi) After updating the state of the photons, we check which of them have reached the free surface or left through the top of the ejection. For all photons that have reached the free surface, the ideal diffuse reflection is applied. If any photons have left the ejection, they are labeled accordingly and removed from subsequent calculations.

(vii) Steps (iii)–(vi) are repeated until all photons have been absorbed or have left the ejection. The frequency shifts of outgoing photons are summarized as the spectrogram.

2.3. Particle models

The MC algorithm indicates that the PDV spectrum is related to the particle size d, velocity v, position z, and number N (*i.e.*, total area mass m_0). This algorithm can be applied in cases where these parameters are completely random. In real situations, however, the particles of the ejecta usually satisfy certain distributions in terms of velocity and diameter.[2,14,15,17,29–32] For the sake of discussion, these assumptions are applied in this paper. Previous studies[2,29] indicate that the initial velocities of particles in the ejecta can be approximated by an exponential law

$$f(v) = \frac{m(v)}{m_0} = \frac{\beta}{v_{fs}} \exp\left[-\beta\left(\frac{v}{v_{fs}} - 1\right)\right], \tag{20}$$

where v_{fs} is the velocity of the free surface and β is the velocity distribution coefficient. Under this exponential law, most of the particles are located in the low-velocity region, which is near the free surface. β determines the non-uniformity of this distribution.

In this paper, we only consider the ejecta in a vacuum environment. After being ejected, the particles retain an almost constant velocity and the ejecta expands in a self-similar manner over time. The particle position z is only related to its initial velocity v and ejection time t_e, $z = vt_e$. The corresponding PDV spectrum exhibits slight changes over time.[21,33]

The particle size distribution is assumed to obey a log-normal law[15,31]

$$n(d) = \frac{1}{\sqrt{2\pi}\sigma d} \exp\left(-\frac{\ln^2(d/d_m)}{2\sigma^2}\right), \tag{21}$$

where σ is the width of the distribution and d_m is the median diameter. These parameters depend on the roughness of the metal surface, shock-induced breakout pressure, and surrounding gas properties. When $\sigma = 0$, the function becomes a Dirac equation and all of the particles have the same diameter. Obviously, this is the ideal situation. The particle distribution can also be described by a power law,[14,30,32] but this description may be invalid in the range of small particle sizes (less than 10 μm).[15] In this paper, the particle size is assumed to be independent of its velocity.

With these assumptions, the determining factors of the PDV spectrum change to the velocity profile coefficient β, total area mass m_0, median diameter d_m, and size distribution width σ. The aim of this paper is to discuss the influence of these parameters on the PDV spectrum, and to explore how they can be extracted from the PDV spectrum most accurately.

2.4. Convergence and comparison

The accuracy of the MC algorithm mainly depends on the initial number of photons. Theoretical PDV spectra with 10^4, 10^5, 10^6, and 10^7 initial photons are shown in Fig. 4. The calculation assumes a vacuum environment and the particles distribution assumptions are applied. In this case, the PDV spectra have a single peak. As the initial number of photons increases, the spectrum curves tend to be smooth. The difference between the spectra with 10^6 and 10^7 initial photons is very slight. Thus, 10^7 initial photons are applied in the following calculations.

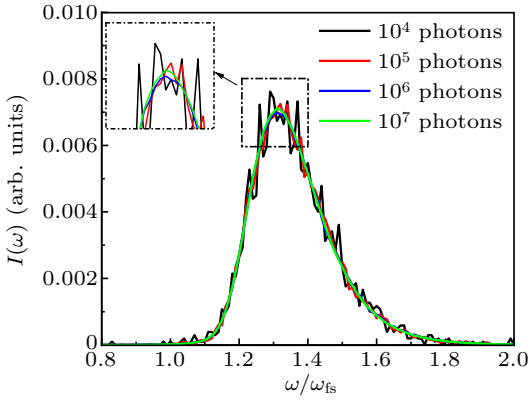


Fig. 4. Theoretical PDV spectra with different initial numbers of photons. The calculation assumes the ejection of Sn particles in a vacuum environment. The particle velocities obey an exponential distribution ($\beta = 10$) and the particle sizes follow a log-normal distribution ($d_m = 1.5$ μm, $\sigma = 0.5$). The total area mass is 20 mg/cm^2. ω_{fs} is the Doppler frequency shift corresponding to the free surface velocity, $\omega_{fs} = 2\omega_r \cdot v_{fs}/c$. The probing wavelength is $\lambda = 1550$ nm.

The high initial number of photons leads to considerable computational cost. For the case of 10^7 photons, a single-core CPU requires approximately 3 h to determine the spectrum. GPUs can be applied to accelerate the calculation. Although the frequency of GPU processors is much lower than that of CPUs, GPUs contain hundreds or thousands of stream processors that can work simultaneously. The acceleration ratio of a GPU compared to a CPU is shown in Fig. 5. The Intel Xeon W-2102 CPU (frequency 2.9 GHz) and two GPUs (Quadro P600 and Nvidia GTX960) are applied. As the initial number of photons increases, the acceleration ratio of the GPUs is enhanced. For the case of 10^7 photons, the acceleration ratio reaches a factor of 8 for the Quadro P600 and a factor of 20 for the Nvidia GTX960. Because there are many judgment events in the procedure, and the GPUs have few logical units, it is difficult to improve the acceleration ratio with these GPUs. Thus, the Nvidia GTX960, which requires approximately 500 s to compute each case, is used in the following calculations.

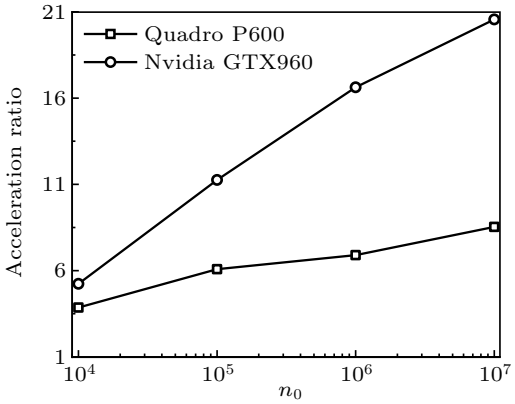


Fig. 5. Acceleration ratio of GPU calculation compared with CPU for different initial numbers of photons. The CPU is an Intel Xeon W-2102 and its basic frequency is 2.9 GHz. The Quadro P600 GPU has 384 stream processors; the clock speed of each processor is about 1.3 GHz. The Nvidia GTX960 GPU has 1024 stream processors; the clock speed of each processor is about 1.1 GHz.

The PDV spectra simulated by the present procedure are compared with those reported by Andriyash *et al*. and Franzkowiak *et al*. in Fig. 6. We use the equivalent ejecta area mass and particle size instead of the transport optical thickness used by Andriyash *et al*. With the uniform scattering assumption, our simulation (case 2) is almost the same as that of Andriyash *et al*. (case 3), which validates the adequacy of the present numerical method. However, when the Mie scattering theory is applied, there is a remarkable difference between the present procedure (case 1) and the results of Andriyash *et al*. (case 3) and Franzkowiak *et al*. (case 4). The difference with Andriyash *et al*. is mainly in the low-velocity part. This is because the change in the scattering phase function has a great influence on the multiple scattering, which is the main form of scattering in the low-velocity dense part. The difference with Franzkowiak *et al*. is in the location of the spectrum peak. Franzkowiak *et al*. applied the single-scattering theory and assumed that all of the light scattered backward. This implies that the optical thickness is overestimated, and so little light would reach the deep region of the ejecta. Thus, the spectrum moves toward high velocities. These differences in spectra indicate that the scattering assumption may introduce some reconstruction inaccuracy that cannot be neglected.

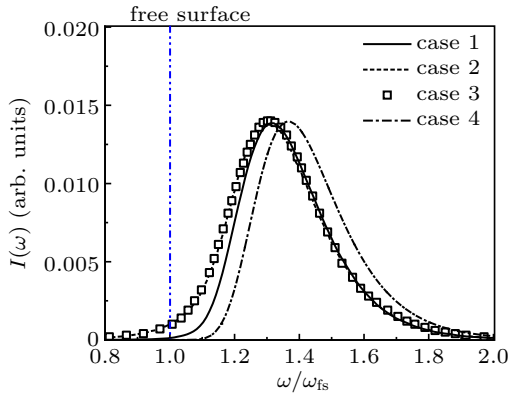


Fig. 6. Comparison of PDV spectra calculated by different reconstruction methods. case 1: MC + Mie scattering theory (proposed procedure); case 2: MC + uniform scattering assumption; case 3: Discrete coordinates + uniform scattering assumption (Andriyash *et al*.); case 4: Single scattering theory (Franzkowiak *et al*.). The data for case 3 were extracted directly from the paper of Andriyash *et al*. The calculations were carried out for a transport scattering thickness of $\tau_{\rm tr} = 10$, which corresponds to $m_0 = 10.7$ mg/cm^2, $d_{\rm m} = 1.5$ μm, and $\sigma = 0.5$. The material is Sn and the ejection velocity profile has $\beta = 8$.

3. Interpretation of PDV spectrum

3.1. Influence of ejecta parameters

The results of numerical calculations that demonstrate the sensitivity of the PDV spectrum to changes in the ejecta parameters (β, m_0, $d_{\rm m}$, and σ) are presented in Figs. 7–10. The PDV spectra were simulated using the MC algorithm described in the previous section for Sn particles in a vacuum environment. The initial ejecta parameters were set to $\beta = 10$, $m_0 = 20$ mg/cm^2, $d_{\rm m} = 1.5$ μm, and $\sigma = 0.5$. In each figure, one of the parameters changes and the others remain constant.

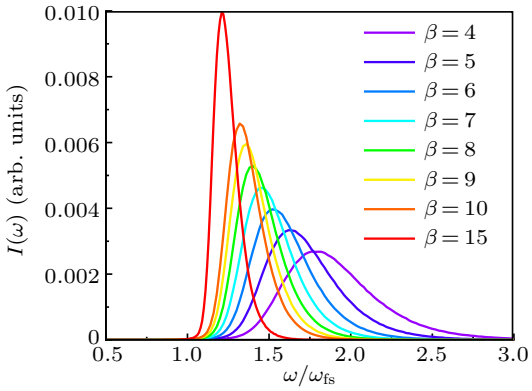


Fig. 7. Simulated PDV spectra with different velocity coefficients. The calculation was carried out for Sn particles in a vacuum environment. The total area mass was 20 mg/cm^2. The log-normal distribution ($d_{\rm m} = 1.5$ μm, $\sigma = 0.5$) was applied to the particle sizes.

The simulated PDV spectra with different values of the velocity coefficient β are shown in Fig. 7. With an increase

in β, the spectrum peak moves towards the low velocities and its magnitude increases. Furthermore, the spectrum shape becomes sharper and the high-velocity part of the spectrum becomes invisible. The coefficient β determines the distribution of particles in the ejecta. With larger β, fewer particles are located at the top of the ejecta and the incident light can penetrate deeper. This results in the movement of the spectrum peak and a decrease in the observability of high-velocity particles.

The simulated PDV spectra with different values of the total area mass m_0 are shown in Fig. 8. The changes in the spectra can be divided into two sections. When $m_0 \geq 10$ mg/cm^2, the spectrum displays a single peak. With a decrease in m_0, this peak moves to the left, and its magnitude and slope exhibit slight changes. When $m_0 \leq 5$ mg/cm^2, a new peak appears around the free surface, and the spectrum exhibits a double-peak shape. A smaller area mass produces a more remarkable new peak. For $m_0 = 2$ mg/cm^2, the original peak disappears and the spectrum again exhibits a single peak. The double-peak spectrum has been observed in previous experiments[18,34] and simulations,[24,35] and is the result of the direct exposure of incident light at the free surface. The detail explanation is shown in Subsection 3.2.

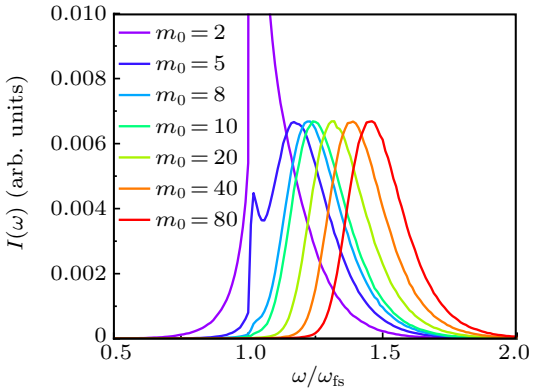


Fig. 8. Simulated PDV spectra with different total area mass. The area mass unit is mg/cm^2. The calculation was carried out for Sn particles in a vacuum environment. The velocity coefficient $\beta = 10$ and the size coefficients $d_{\rm m} = 1.5$ μm, $\sigma = 0.5$.

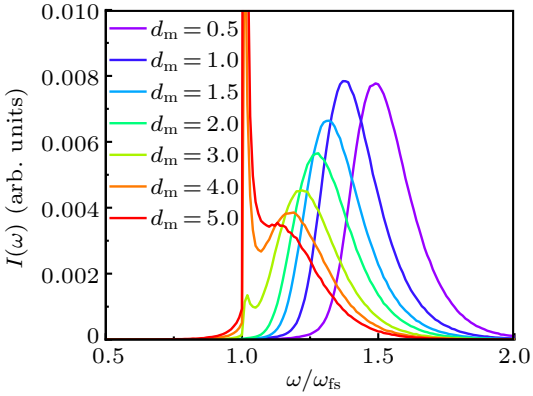


Fig. 9. Simulated PDV spectra with different particle median diameters. The diameter unit is μm. The calculation was carried out for Sn particles in a vacuum environment. The total area mass was 20 mg/cm^2. The velocity coefficient $\beta = 10$ mg/cm^2 and the size coefficient $\sigma = 0.5$.

There are two parameters that determine the particle size distribution — the median diameter $d_{\rm m}$ and the distribution width σ. Their influence on the PDV spectrum is illustrated in Figs. 9 and 10, respectively. $d_{\rm m}$ and σ exhibit similar effects: as $d_{\rm m}$ or σ increases, the original peak of the spectrum moves towards the low velocities and the peak value decreases. A new peak then appears in the position of the free surface and the original peak gradually attenuates. This change in the form of the spectrum peak is similar to that for the area mass.

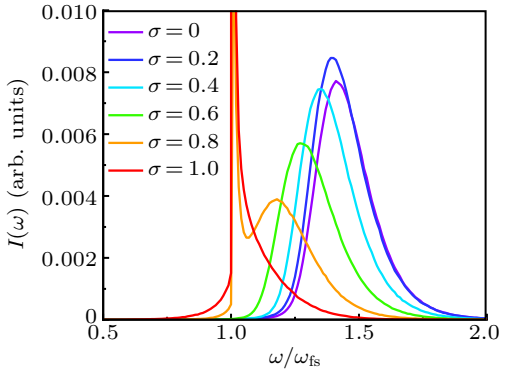


Fig. 10. Simulated PDV spectra with different particle size coefficients σ. The calculation was carried out for Sn particles in a vacuum environment. The total area mass was 20 mg/cm^2. The velocity coefficient $\beta = 10$ and the median diameter $d_{\rm m} = 1.5$ μm.

3.2. Theoretical optical model

The simulations described above using the MC algorithm provide a qualitative understanding of the influence of the ejecta parameters on the PDV spectrum. However, how to solve the reverse problem, *i.e.*, extracting the ejecta parameters from the PDV spectrum, remains unclear. To obtain the quantitative relationships between the ejecta parameters and the characteristics of the PDV spectrum, we introduce the single-scattering theory. In this theory, the light is assumed to be scattered only once, and the scattering direction is always backward. With this assumption, the light direction is always parallel to the motion of the particles. The frequency shift of the light is proportional to the particle velocity, $\omega = 2\omega_0 \cdot v/c$. The PDV spectrum can be expressed in terms of velocity, $I(\tilde{v})$.

The above calculations have shown that the single scattering leads to an overestimation of the optical thickness. Here, we assume that the extinction process of particles only includes the backscattering and absorption effects, and the forward scattering is ignored. With this assumption, the PDV spectrum is calculated by the formula

$$\begin{aligned} I(\omega) = I(\tilde{v}) &\propto \sum_{i}^{\tilde{v}<v<\tilde{v}+dv} \sqrt{I_{{\rm back},i}} \\ &= \sum_{i}^{\tilde{v}<v<\tilde{v}+dv} \sqrt{\frac{I_0}{A_{\rm s}} A_{{\rm back},i}(v) \cdot \exp\left(-2\int_{\tilde{v}}^{\infty} \tau(v)\,{\rm d}v\right)} \\ &\propto \sum_{i}^{\tilde{v}<v<\tilde{v}+dv} \sqrt{A_{{\rm back},i}(v)} \cdot \sqrt{\exp\left(-2\int_{\tilde{v}}^{\infty} \tau(v)\,{\rm d}v\right)}, \end{aligned} \quad (22)$$

where $\tilde{v}$ is the velocity corresponding to the frequency shift, $\tilde{v} = 2\omega c/\omega_{\rm r}$, and $A_{\rm back}$ is the backscattering cross-section area of particles with velocity $\tilde{v}$:

$$\begin{aligned}\sum_{i}^{\tilde{v}<v<\tilde{v}+dv}\sqrt{A_{{\rm back},i}(v)} &= \sum_{i}^{\tilde{v}<v<\tilde{v}+{\rm d}v}\sqrt{\frac{1}{4}\pi d_i^2 K_{\rm back}} \\ &= N(\tilde{v})\frac{1}{2}\bar{d}\sqrt{\pi K_{\rm back}} = \frac{m(\tilde{v})A_{\rm s}}{(1/6)\pi\overline{d^3}\rho_0}\frac{1}{2}\bar{d}\sqrt{\pi K_{\rm back}} \\ &= \frac{3A_{\rm s}\sqrt{K_{\rm back}}}{\sqrt{\pi}\rho_0}\frac{m_0}{\overline{d^3}/\bar{d}}f(\tilde{v}),\end{aligned} \tag{23}$$

where $\bar{d}$ is the average particle diameter and $K_{\rm back}$ is the backscattering coefficient, which is calculated by Mie theory.

The exponent in Eq. (22) denotes the extinction effects, where the coefficient 2 signifies the back and forth of light in the ejection process. The integral represents the contributions from the extinction of particles above the layer of velocity $\tilde{v}$:

$$\begin{aligned}\int_{\tilde{v}}^{\infty}\tau(v){\rm d}v &= \frac{\sum_{i}^{v>\tilde{v}}(\pi/4)d_i^2K_{\rm ext}^*}{A_{\rm s}} = \frac{\int_{\tilde{v}}^{\infty}N(v){\rm d}v\cdot(\pi/4)\overline{d^2}K_{\rm ext}^*}{A_{\rm s}} \\ &= \frac{3K_{\rm ext}^*}{2\rho_0}\frac{\int_{\tilde{v}}^{\infty}m(v){\rm d}v}{\overline{d^3}/\overline{d^2}},\end{aligned} \tag{24}$$

where the equivalent extinction coefficient $K_{\rm ext}^*$ only considers the backscattering and absorption effects:

$$K_{\rm ext}^* = K_{\rm back} + K_{\rm abs} = g_{\rm back}K_{\rm ext}, \tag{25}$$

where the coefficient $g_{\rm back}$ is 0.5–0.7 for particle diameters of 1 μm–10 μm. When $g_{\rm back} = 1$, the present model reduces to that of Franzkowiak *et al*.

Because the velocity profile is exponential, $\int_{\tilde{v}}^{\infty}m(v){\rm d}v = m_0 f(\tilde{v})v_{\rm fs}/\beta$. Equation (25) has the form

$$\int_{\tilde{v}}^{\infty}\tau(v){\rm d}v = \frac{3K_{\rm ext}^*}{2\rho_0}\frac{m_0}{\overline{d^3}/\overline{d^2}}\frac{v_{\rm fs}}{\beta}f(v), \tag{26}$$

When $\tilde{v}$ is equal to the free surface velocity, the integral represents the amount of light that is able to reach the free surface. The optical thickness of the ejecta is defined as

$$\tau_0 = \int_{v_{\rm fs}}^{\infty}\tau(v){\rm d}v = \frac{3K_{\rm ext}^*}{2\rho_0}\frac{m_0}{\overline{d^3}/\overline{d^2}}. \tag{27}$$

Combining Eqs. (23), (26), and (27), we can write Eq. (22) as

$$I(\tilde{v}) \propto \frac{\sqrt{K_{\rm back}}}{K_{\rm ext}^*}\cdot\frac{\bar{d}}{\overline{d^2}}\cdot\tau_0 f(\tilde{v})\exp\left(-\frac{v_{\rm fs}}{\beta}\tau_0 f(\tilde{v})\right). \tag{28}$$

This equation provides the theoretical form for determining the PDV spectrum from the ejecta parameters in a vacuum environment. In this formula, the PDV spectrum is proportional to the product of the velocity profile and the extinction term. These two parts are illustrated in Fig. 11. As the velocity decreases, the corresponding ejecta position moves closer to the free surface, and the incident light becomes weaker because of particle extinction. However, the particles become dense deeper within the ejecta, and this enlarges the cross-section area of scattering. With the contribution of these two parts, the PDV spectrum exhibits a single peak shape.

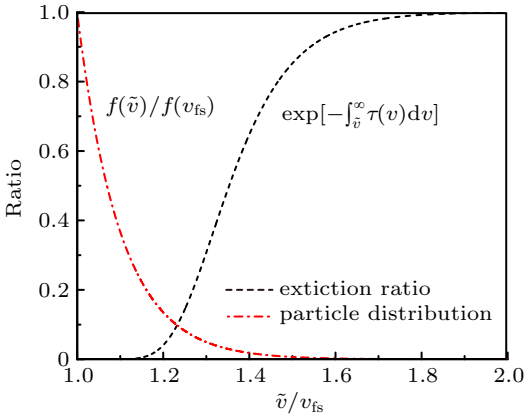


Fig. 11. Extinction ratio and particle distribution with respect to velocity.

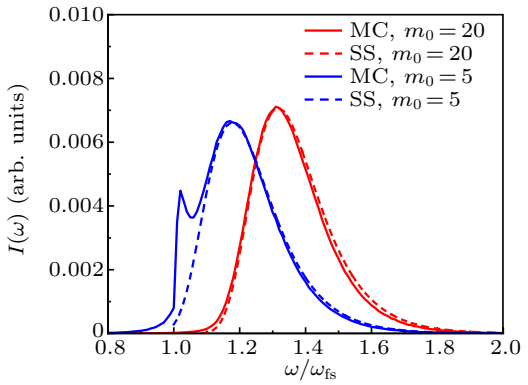


Fig. 12. Simulated PDV spectrum by MC algorithm and single-scattering (SS) model. The area mass unit is mg/cm^2. The particle settings are $\beta = 10$, $d_{\rm m} = 1.5$ μm, $\sigma = 0.5$. The backscattering coefficient is $g_{\rm back} = 0.67$.

The simulated PDV spectra of the present model are compared with those of the MC algorithm in Fig. 12. With the correction of the backscattering coefficient, there is a good agreement between the results, both in the main peak position and the curve shape. This agreement is resulted by the slight multiple scattering effects in ejecta field. According to the Mie theory, most of scattering light is forward with the particle diameter 1 μm–10 μm. So multiple scattering rarely occurs, and the single scattering theory can describe the PDV spectrum very well. However, in the case of a small ejecta mass ($m_0 = 5$ mg/cm^2), the present model cannot simulate the peak around the free surface. From the Eq. (22), the spectrum value in a certain velocity is related to the backscattering section and the local light intensity. In the free surface, most photons are scattered backward and the backscattering section is much larger than that of the particles, which results the new spectrum peak near the free surface. In the present model, the backscattering of incident light on the free surface is ignored, so there is no spectrum peak near the free surface in the case of a small ejecta mass ($m_0 = 5$ mg/cm^2). Even so, we mainly

consider the information supplied by the original peak of the PDV spectrum in this paper. Thus, this defect has only a very slight influence on the accuracy of the present model.

We now analyze the spectrum function [Eq. (28)]. First, we take its derivative

$$I'(\tilde{v}) \propto \tau_0 f'(\tilde{v}) \exp\left(-\frac{v_{\rm fs}}{\beta}\tau_0 f(\tilde{v})\right)\left(1-\frac{v_{\rm fs}}{\beta}\tau_0 f(\tilde{v})\right)$$
$$= -\frac{\beta}{v_{\rm fs}} I(\tilde{v})\left(1-\frac{v_{\rm fs}}{\beta}\tau_0 f(\tilde{v})\right), \quad (29)$$

where $f'(\tilde{v}) = -\beta/v_{\rm fs} f(\tilde{v})$.

When $I'(\tilde{v}) = 0$, the solution provides the position of the spectrum peak

$$1-\frac{v_{\rm fs}}{\beta}\tau_0 f\left(\tilde{v}_{\rm peak}\right) = 0, \quad (30)$$
$$\tilde{v}_{\rm peak}/v_{\rm fs} = 1+\ln(\tau_0)/\beta. \quad (31)$$

The peak value of the PDV spectrum is

$$I\left(\tilde{v}_{\rm peak}\right) \propto \frac{\sqrt{K_{\rm back}}}{K^*_{\rm ext}} \cdot \frac{\bar{d}}{\overline{d^2}} \cdot \frac{\beta}{v_{\rm fs}} {\rm e}^{-1} \propto \frac{\beta}{\overline{d^2}/\bar{d}}. \quad (32)$$

Finally, the relative curvature at the spectrum peak is given by the second derivative of the spectrum function

$$I''(\tilde{v})/I\left(\tilde{v}_{\rm peak}\right) = \frac{v_{\rm fs}}{\beta} e\left(\tau_0 f(\tilde{v}) \exp\left(-\frac{v_{\rm fs}}{\beta}\tau_0 f(\tilde{v})\right)\right)', \quad (33)$$
$$I''\left(\tilde{v}_{\rm peak}\right)/I\left(\tilde{v}_{\rm peak}\right) = -\left(\frac{\beta}{v_{\rm fs}}\right)^2. \quad (34)$$

In summary, the relationships between the ejecta parameters and the characteristics of the PDV spectrum have the form

$$\begin{cases} \tilde{v}_{\rm peak}/v_{\rm fs} = 1+\ln(\tau_0)/\beta, \\ I\left(\tilde{v}_{\rm peak}/v_{\rm fs}\right) \propto \dfrac{\beta}{\overline{d^2}/\bar{d}}, \\ I''\left(\tilde{v}_{\rm peak}/v_{\rm fs}\right)/I\left(\tilde{v}_{\rm peak}/v_{\rm fs}\right) = -\beta^2, \end{cases} \quad (35)$$

where the independent variable is normalized by the velocity of the free surface, $v_{\rm fs}$.

The above relationships allow some of the ejecta parameters to be determined. First, the velocity profile coefficient β is given by the relative curvature at the spectrum peak. In addition, the surface mean diameter $d^* = \overline{d^2}/\bar{d} = d_{\rm m}\,{\rm e}^{0.5\sigma^2}$ can be derived from the value of the spectrum peak. Finally, the optical thickness of the ejecta τ_0 is obtained from the position of the spectrum peak, where τ_0 is related to the ejecta area mass m_0 and the Sauter mean diameter $d_{\rm s} = \overline{d^3}/\overline{d^2} = d_{\rm m}\,{\rm e}^{2.5\sigma^2}$. If $d_{\rm s}$ is assumed to be approximately d^*, the area mass m_0 can be determined.

It is worth nothing that the relationship (Eq. (35)) has some limitation. When the optical thickness is sufficiently small and the original peak disappears, it is hard to obtain the correct spectrum peak value and curvature. In this case, the ejecta parameter extraction method will be invalid.

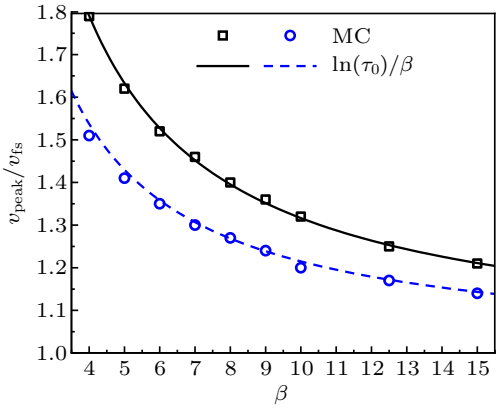


Fig. 13. Peak positions of PDV spectrum calculated by MC algorithm and theoretical formula. Two optical thickness are considered, where the square points denote $\tau_0 = 23.4$ and the circular points denote $\tau_0 = 8.6$. The corresponding ejecta parameters are $m_0 = 20$ mg/cm^2, $d_{\rm m} = 1.5$ μm, $\sigma = 0.5$ and $m_0 = 10$ mg/cm^2, $d_{\rm m} = 2.0$ μm, $\sigma = 0.5$, respectively.

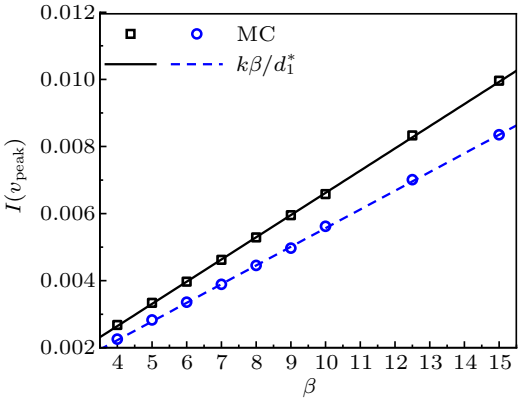


Fig. 14. Peak values of PDV spectrum calculated by MC algorithm and theoretical formula. Two optical thicknesses are considered, where the square points denote $\tau_0 = 23.4$ and the circular points denote $\tau_0 = 8.6$. The corresponding ejecta parameters are $m_0 = 20$ mg/cm^2, $d_{\rm m} = 1.5$ μm, $\sigma = 0.5$ and $m_0 = 10$ mg/cm^2, $d_{\rm m} = 2.0$ μm, $\sigma = 0.5$, respectively.

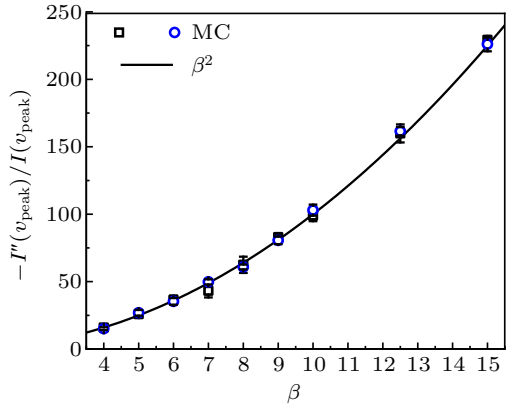


Fig. 15. Relative curvature of PDV spectrum at the peak calculated by MC algorithm and theoretical formula. Two optical thickness are considered, where the square points denote $\tau_0 = 23.4$ and the circular points denote $\tau_0 = 8.6$. The corresponding ejecta parameters are $m_0 = 20$ mg/cm^2, $d_{\rm m} = 1.5$ μm, $\sigma = 0.5$ and $m_0 = 10$ mg/cm^2, $d_{\rm m} = 2.0$ μm, $\sigma = 0.5$, respectively.

Figures 13–15 compare these theoretical relationships with the MC simulation results. Two optical thickness and a large range of velocity profiles are considered. In the cases of $\tau_0 = 23.4$, the PDV spectra have single peak, and in the case of $\tau_0 = 8.6$, the PDV spectra have double-peak. They are two

typical types of PDV spectra. It can be observed that the theoretical relationships largely conform to the MC simulations in these cases, which verifies the present model to some extent.

3.3. Experimental verification

In the above relationships, the peak value of the spectrum is difficult to use in the analysis of PDV experiments. In the experiments, the PDV spectrum is scaled by the reference light intensity, probe reception, photoelectric conversion efficiency, and circuit amplification factor, among other factors. Additional PDV experiments are required to calibrate this scaled factor. For a single PDV vacuum experiment, only the velocity profile β and optical thickness τ_0 of the ejecta can be extracted. If there is an additional particle granularity measurement, the ejecta area mass m_0 can also be determined.

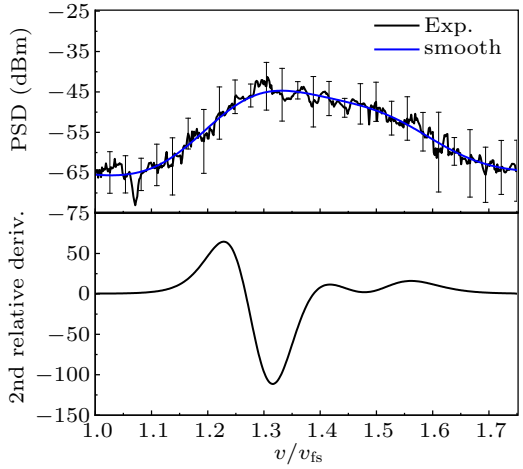


Fig. 16. (a) PDV spectrogram extracted from ejecta experiment of Franzkowiak *et al.*[21] and (b) second derivative (deriv.) of the smooth data.

A set of ejecta PDV experiments performed by Franzkowiak *et al.*[21] was used to verify the present theoretical model. The experiment was carried out in a vacuum environment using Sn material with the surface machined into 60 μm×8 μm grooves. The shock-induced breakout pressure was $P_{\rm SB} = 28$ GPa. The velocity of the free surface was found to be approximately 2013 m/s. We extracted the PDV spectrum from the experimental spectrogram over the period 0.2 μs–0.8 μs, as shown in Fig. 16(a). The PDV data were then averaged and smoothed using the low-pass filtering of the fast Fourier transform. We converted the spectrum units [dBm] to volts and then took the second derivative to give the smoothed PDV spectrum shown in Fig. 16(b). The peak of this spectrum is located at $\tilde{v}/v_{\rm fs} = 1.32$ and the corresponding relative curvature is approximately -110. Combined with Eq. (35), this suggests a velocity profile coefficient of $\beta = 10.5$ and an optical thickness of $\tau_0 = 28.79$. Depending on the frequency of the filter, the errors of the extracted parameters are within 10%.

Schauer *et al.*[31] conducted a Mie-scattering experiment with similar conditions, where the surface roughness was 50 μm×8 μm and the breakout pressure was about 30 GPa. The particle size distribution was measured to be $d_{\rm m} = 0.6$ μm, $\sigma = 0.5$. Using this data, the total area mass was determined to be $m_0 = 7.5$ mg/cm^2.

In their PDV experiment, Franzkowiak *et al.* simultaneously measured the area mass with respect to velocity using a piezoelectric probe. The PDV spectrum and area mass given by our estimations and their experiments are compared in Figs. 17 and 18, respectively. These two results are in good agreement, which verifies the present theoretical model.

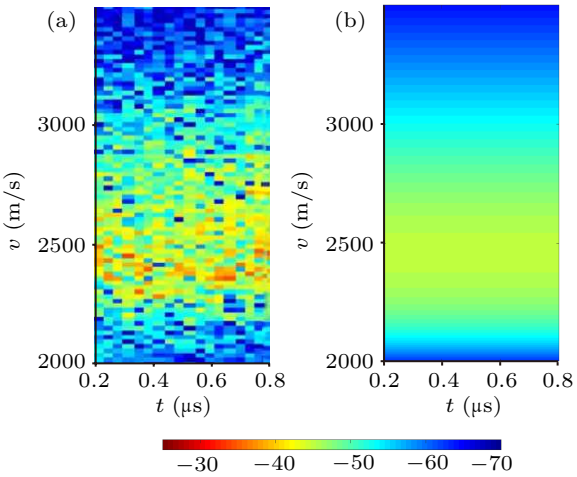


Fig. 17. Comparison of the experimental and simulated PDV spectra.

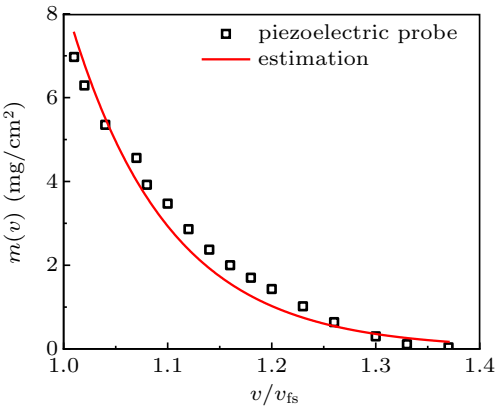


Fig. 18. Comparison of the area mass and velocity profile between the piezoelectric probe measurement[21] and our estimation.

4. Conclusion

This paper has discussed the PDV spectrum of ejecta particles from shock-loaded samples in a vacuum. A GPU-accelerated MC algorithm that rebuilds the PDV spectrum for the ejecta particles has been proposed, and Mie theory was applied to describe the scattering process. Compared with the reconstruction methods of Andriyash *et al.* and Franzkowiak *et al.*, a reasonable scattering model is the key to simulating the PDV spectrum accurately. The influences of particle velocity profile, particle size and ejecta area mass on PDV spectrum are discussed, and two typical types of the PDV spectrum

are found: single-peak and double-peak. For a quantitative analysis, a corrected single-scattering model is proposed for deriving the relationships between the ejecta parameters and the characteristics of the PDV spectrum. Based on the relationships, the ejecta parameters β, d, and m_0 can be extracted from the PDV spectrum directly. The theoretical relationships and estimated parameters are found to be in good agreement with the MC simulations and PDV experiments of ejecta in a vacuum environment.

The present theoretical model still has some limitation. The particles considered in this paper are in the diameter of 1 μm–10 μm, and the multiple scattering effects are very slight. If the particle diameter is smaller than this range, the multiple scattering effects must be considered. The spectrum reconstruction algorithm is still available, but the simplified theoretical model may be valid. In addition, the parameter extraction method is based on the original main peak. If the optical thickness is sufficiently small and the original peak disappears, the relationships between ejecta parameters and spectrum information will be hard to be utilized. How to determine the particle size in the PDV experiment is another unsolved issue. In future work, more experimental results will be used to verify the present model, and the PDV spectrum in gas environment will be discussed in an attempt to recover more comprehensive quantities of the ejecta.

References

[1] Sollier A and Lescoute E 2020 *Int. J. Impact Eng.* **136** 103429
[2] Monfared S K, Oro D M, Graver M, Hammerberg J E, Lalone B M, Pack C L, Schauer M M, Stevens G D, Stone J B and Turley W D 2014 *J. Appl. Phys.* **116** 063504
[3] Asay J R, Mix L P and Perry F C 1976 *Appl. Phys. Lett.* **29** 284
[4] Speight C S, Harper L and Smeeton V S 1989 *Rev. Sci. Instrum.* **60** 3802
[5] Ogorodnikov V A, Ivanov A G, Mikhailov A L, Kryukov N I and Golubev V A 1998 *Combust. Explos. Shock Waves* **34** 696
[6] Buttler W T, Williams R J R and Najjar F M 2017 *J. Dyn. Behav. Mater.* **3** 151
[7] Yeager J D, Bowden P R, Guildenbecher D R and Olles J D 2017 *J. Appl. Phys.* **122** 035901
[8] Held M 1996 *Propellants Explos. Pyrotech.* **21** 235
[9] Tokheim R E, Curran D R, Seaman L, Cooper T and Schirmann D 1999 *Int. J. Impact Eng.* **23** 933
[10] Masters N D, Fisher A, Kalantar D, Stlken J, Smith C, Vignes R, Burns S, Doeppner T, Kritcher A and Park H S 2016 *J. Phys.: Conf. Ser.* **717** 012108
[11] Asay J R 1978 *J. Appl. Phys.* **49** 6173
[12] He W, Xin J, Chu G, Li J and Gu Y 2014 *Opt. Express* **22** 18924
[13] Vogan W S, Anderson W W, Grover M, Hammerberg J E, King N S P, Lamoreaux S K, Macrum G, Morley K B, Rigg P A and Stevens G D 2005 *J. Appl. Phys.* **98** 113508
[14] Sorenson D S, Minich R W, Romero J L, Tunnell T W and Malone R M 2002 *J. Appl. Phys.* **92** 5830
[15] Sorenson D S, Capelle G A, Grover M, Johnson R P and Turley W D 2017 *J. Dyn. Behav. Mater.* **3** 233
[16] Hammerberg J E, Buttler W T, Llobet A, Morris C, Goett J, Manzanares R, Saunders A, Schmidt D, Tainter A and Vogan-Mcneil W 2018 *AIP Conf. Proc.* **1979** 080006
[17] Monfared S K, Buttler W T, Frayer D K, Grover M, LaLone B M, Stevens G D, Stone J B, Turley W D and Schauer M M 2015 *J. Appl. Phys.* **117** 223105
[18] La-Lone B M, Marshall B R, Miller E K, Stevens G D, Turley W D and Veeser L R 2015 *Rev. Sci. Instrum.* **86** 023112
[19] Ogorodnikov V A, Mikhaylov A L, Erunov S V, Antipov M V and Chudakov E A 2017 *J. Dyn. Behav. Mater.* **3** 225
[20] Andriyash A V, Astashkin M V, Baranov V K, Golubinskii A G, Irinichev D A, Khatunkin V Y, Kondratev A N, Kuratov S E, Mazanov V A, Rogozkin D B and Stepushkin S N 2018 *J. Appl. Phys.* **123** 243102
[21] Buttler W T, Oro D M, Dimonte G, *et al.* 2009 *In Proceedings NEDPC 2009.* LA-UR-10-00734
[22] Sun H, Wang P, Chen D and Ma D 2016 *Acta Phys. Sin.* **65** 104702 (in Chinese)
[23] Fedorov A V, Gnutov I S and Yagovkin A O 2018 *J. Exp. Theor. Phys.* **126** 76
[24] Kondrat'Ev A, Andriyash A V and Kuratov S E 2020 *J. Quantum Spectrosc. Radiat. Transfer* **246** 106925
[25] Buttler W T, Oro D M, Dimonte G, *et al.* 2009 In *Proceedings NEDPC* 2009, LA-UR-10-00734
[26] Reguigui N M, Ackerson B J, Dorri-Nowkoorani F, Dougherty R L and Nobbmann U 1997 *J. Thermophys. Heat Transfer* **11** 400
[27] Binzoni T, Liemert A, Kienle A and Martelli F 2016 *Appl. Opt.* **55** 8500
[28] Mie G 1908 *Ann. Phys.* **25** 377
[29] Durand O and Soulard L 2015 *J. Appl. Phys.* **117** 165903
[30] Durand O and Soulard L 2012 *J. Appl. Phys.* **111** 044901
[31] Schauer M M, Buttler W T, Frayer D K, Grover M and Turley W D 2017 *J. Dyn. Behav. Mater.* **3** 217
[32] He A, Wang P, Shao J and Duan S 2017 *Chin. Phys. B* **23** 047102
[33] Bell D J, Routley N R, Millett J C F, Whiteman G and Keightley P T 2017 *J. Dyn. Behav. Mater.* **3** 208
[34] Andriyash A V, A D S, Zhakhovskya V V, Kalashnikovc D A, Kondrateva A N, Kuratova S E, Mikhailovc A L, Rogozkina D B, Fedorovc A V, Finyushinc S A and Chudakovc E A 2020 *J. Exp. Theor. Phys.* **130** 338
[35] Franzkowiak J E, Mercier P, Prudhomme G and Berthe L 2018 *Appl. Opt.* **57** 11